Polarization measurements at X- and gamma-ray energies:

expectation of emission models clarification?, or, of just another confusion?

A.F. Iyudin

**Skobeltsyn Institute of Nuclear Physics,
Lomonosov Moscow State University,
Moscow, Russian Federation**

X-ray Polarization in Astrophysics

Stockholm, Sweden, 25-28 August, 2014

Theoretical justification of polarimetry

Theoretical estimates of X-ray polarization for astrophysical sources and emission mechanisms were made by:

Synchrotron	Westfold (1959)
Non-thermal Bremsstrahlung	Brown (1971)
Magnetic Field	Gnedin & Sunyaev (1974)
Binary systems	Rees (1975)
General Relativity	Starck & Connors (1977)
Scattering	Sunyaev & Titarchuk (1985)
AXPs	Viironen & Poutanen (2004)
……	……

Early achievements of polarimetry!!!

1970: First measurements of polarization for non-thermal bremsstrahlung of solar flares by instruments on-board "Intercosmos-1"
Tindo et al. (1970), Solar Physics, v. 14, p. 204

1972: First non-solar astronomical X-ray polarization measurements (Aerobee 350 rocket, Crab Nebula)
Novick et al. (1972);

1972: More polarization results for October/November 1970 solar flares measured on-board "Intercosmoc-4"- P&PA --varied
Tindo et al. (1972), Solar Physics, v. 24, pp. 429-433.

1976: First successful X-ray polarization measurement of Crab Nebula (OSO-8)
Weisskopf et al. (1976)!

The early rocket experiments

- 1968 Aerobee 150
  - Sco X-1 upper limit
- 1969 Aerobee 150
  - Crab upper limit

Novick et al. (1972)

- 1971 Aerobee 350
  - Crab detection!
    - P = 15% ± 5%
    - φ = 156° ± 10°

The satellite experiment

Weisskopf et al. (1976; 1978)

- 1975 OSO-8 satellite
  - Precision measurement of Crab Nebula
    - $\prod = 19\% \pm 1\%$
    - $\varphi = 156° \pm 2°$ (NNE)

Weisskopf et al. (1978) – very good treatment of the background problem

TABLE 1

Parameter*	First Order (2.6 keV) Signal Plus Background	First Order (2.6 keV) Background: Earth Occulted	First Order (2.6 keV) Background: Off Source	Second Order (5.2 keV) Signal Plus Background	Second Order (5.2 keV) Background: Earth Occulted	Second Order (5.2 keV) Background: Off Source
			1976 Observation			
$\bar{R}$ (Counts $s^{-1} \times 10^3$)	343.17 ± 1.59	40.33 ± 0.63	39.07 ± 0.48	78.87 ± 0.77	26.23 ± 0.50	27.24 ± 0.40
X (Counts $s^{-1} \times 10^3$)	39.30 ± 2.25	3.80 ± 0.89	1.42 ± 0.68	5.80 ± 1.09	0.13 ± 0.71	-0.23 ± 0.57
Y (Counts $s^{-1} \times 10^3$)	-37.75 ± 2.25	-0.04 ± 0.89	1.28 ± 0.68	-7.95 ± 1.09	0.93 ± 0.71	-1.07 ± 0.57
A (Counts $s^{-1} \times 10^3$)	54.49 ± 3.35	3.80 ± 1.33	1.91 ± 1.01	9.84 ± 1.63	$0.94 \pm {1.05 \atop 0.94}$	1.10 ± 0.85
a (%)	15.88 ± 0.98	9.42 ± 3.29	4.89 ± 2.59	12.48 ± 2.06	$3.58 \pm {4.01 \atop 3.58}$	4.02 ± 3.09
ϕ (degrees)	158.08 ± 1.77	179.70 ± 9.63	21.02 ± 13.95	153.06 ± 4.69	$41.02 \pm {138.98 \atop 41.02}$	128.94 ± 18.77
			1977 Observation			
$\bar{R}$ (Counts $s^{-1} \times 10^3$)	336.24 ± 2.13	32.90 ± 0.34	38.76 ± 0.53	77.81 ± 1.00	21.38 ± 0.29	24.64 ± 0.41
X (Counts $s^{-1} \times 10^3$)	36.67 ± 3.01	0.59 ± 0.48	-0.19 ± 0.75	5.34 ± 1.41	0.22 ± 0.41	0.34 ± 0.58
Y (Counts $s^{-1} \times 10^3$)	-42.13 ± 3.01	-0.88 ± 0.48	0.14 ± 0.75	-7.96 ± 1.41	0.25 ± 0.41	-0.43 ± 0.58
A (Counts $s^{-1} \times 10^3$)	55.85 ± 4.48	1.06 ± 0.72	$0.24 \pm {4.94 \atop 0.24}$	9.59 ± 2.10	$0.33 \pm {0.61 \atop 0.33}$	$0.55 \pm {0.87 \atop 0.55}$
a (%)	16.61 ± 1.33	3.22 ± 2.18	$0.61 \pm {2.88 \atop 0.61}$	12.33 ± 2.71	$1.56 \pm {2.86 \atop 1.56}$	$2.22 \pm {3.5 \atop 2.22}$
ϕ (degrees)	155.52 ± 2.29	151.92 ± 17.05	$71.81 \pm {108.19 \atop 71.81}$	151.93 ± 6.20	$24.33 \pm {155.67 \atop 24.33}$	$154.17 \pm {25.83 \atop 154.17}$

*$\bar{R}$ is the average counting rate. X and Y are the components of modulation with positive X and Y measured in the north and east directions, respectively. A is the amplitude of modulation. The fractional amplitude of modulation a is $(X^2 + Y^2)^{1/2}/\bar{R}$, and the position angle $\phi = \frac{1}{2} \tan^{-1}(Y/X)$, measured positive east from north. The errors in a and ϕ are the extremes on the 67% confidence contours.

Weisskopf, et al., ApJ (1978)

Polarimetry is difficult

- One does not expect all astrophysical systems to be strongly polarized.

- Instruments typically not fully sensitive to polarization

- Measured parameter is positive definite – i.e. one always measures something, even in the absence of a polarized source.

Polarization measured depends upon:

Source morphology;
Strength of the source signal;
Geometry of the reprocessing material;
Strength and ordering of the local magnetic field;
Strength and ordering of the LOS fields;
Instrument signal to noise ratio

But! We need polarimetry !!!

- Polarimetry is powerful tool
- Polarimetry needs to be done!
- Theorists have to continue to predict!
- Different objects have to be realistically evaluated as targets for phase resolved polarimetry! Simulations+ Calibrations!

New history of polarization observations

1. Recent : RHESSI (McConnell et al. (2002))
2. The present : INTEGRAL (more below) and GAP,

   see paper by Toma et al. (2013), and talk by Yonetoku)

3. The future : Astro-H, ETCCs (Smile-III ?), GEMS,

   GROME, IXPE, PheniX, POET, PoGO, POLAR,

   X-Calibur, XIPE, XTP, other missions … ???

Objects to study

XIPE selection:

- Acceleration phenomena:
  - SNRs
  - PWNs
  - Jets
  - Magnetic reconnection
- Emission in strong magnetic fields:
  - Accreting WDs
  - MS pulsars
  - Accreting pulsars
- Scattering in aspherical geometries:
  - XRBs
  - Radio-quiet AGNs
  - X-ray reflection nebulae

SNRs as acceleration sites

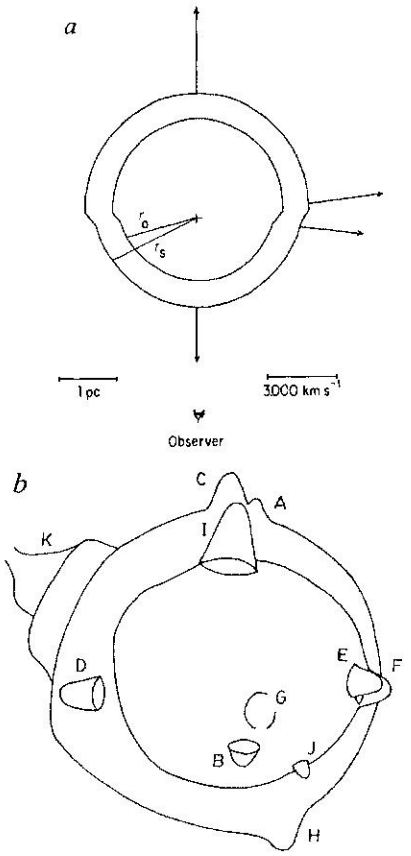

Fig. 2 *a*, First-order geometrical model of Cas A viewed from above the galactic plane, as derived from optical and radio dynamical data (see ref. 2). The vectors indicate the current velocity of the outer shock, while the surfaces at r_0 and r_s represent the locations of the reverse and outer shocks respectively. *b*, Sketch of major shell and bow-shock features identified in the current program of radio imaging. The limb-brightened revese shock interface (r_0 in Fig. 2*a*) of the smaller front hemisphere is seen in projection against the rear hemisphere. Paraboloid extensions labelled A–K are visible as they propagate in the zone of enhanced particle and energy density betwen this surface and the outer shock (at r_s).

Table 2 Bow-shock parameters

Feature	Minimum μ_{obs}	Ellipticity	Estimated μ_0	Mach number
A	28°	~0	28°	2.1
B	22.5°	0.68	17°	3.4
C	26°	~0	26°	2.3
D	11.5°	0.43	10.5°	5.5
E	20°	0.38	18.5°	3.1
F	20°	0.25	19°	3.1
G	—	~1	—	—
H	31.5°	~0	31.5°	1.9
I	20.5°	0.29	19.5°	3.0
J	13°	0.29	12.5°	4.6
K	21.5°	~0	21.5°	2.7

Braun, Gull, Perley, ApJ (1987)

Cas A as acceleration site

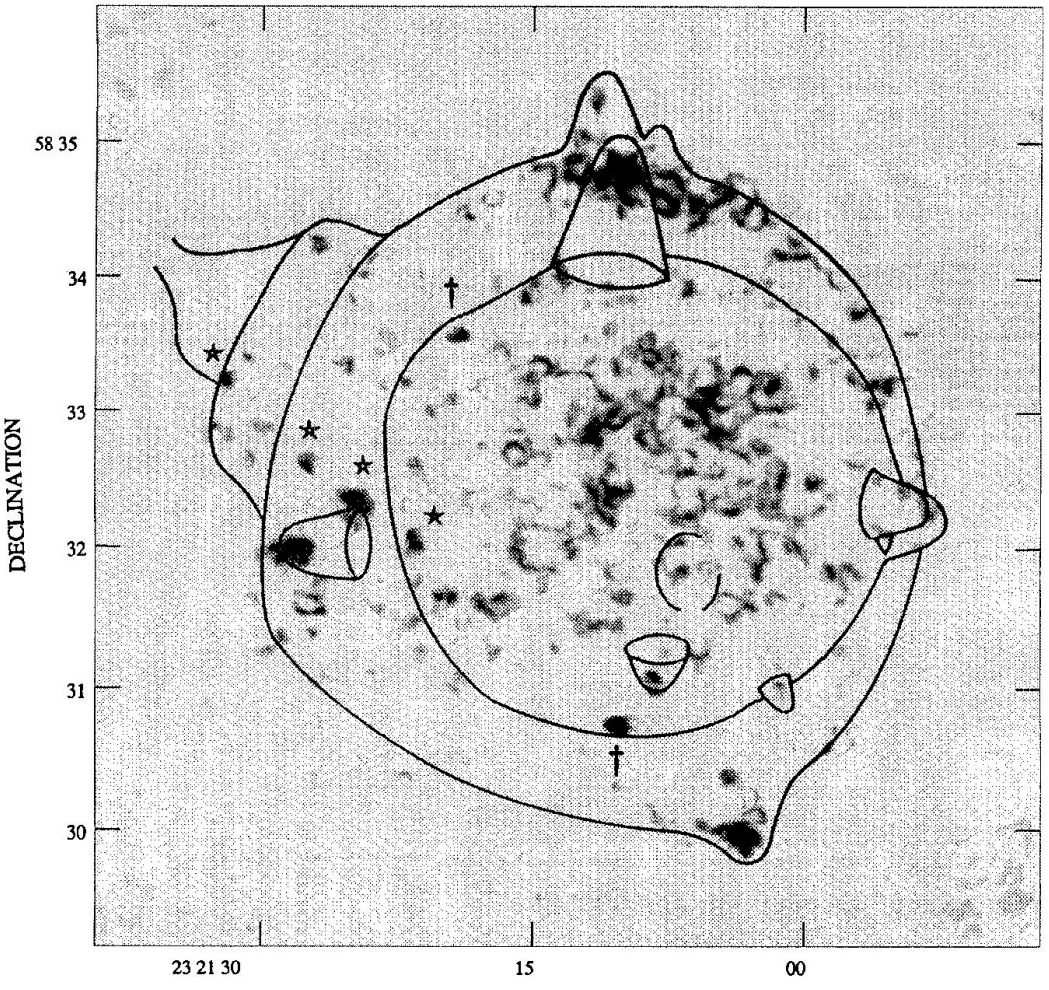

FIG. 9.—Difference between post- and preconvolved images of polarized intensity (see discussion in text). Overlaid are schematics demarcating BGP's 11 "bow shocks" (*solid lines*; from BGP) and symbols identifying new features discussed here.

ANDERSON, KEOHANE, & RUDNICK (see 441, 305)

Anderson, Keohane, Rudnick (1995)

Cas A as acceleration site

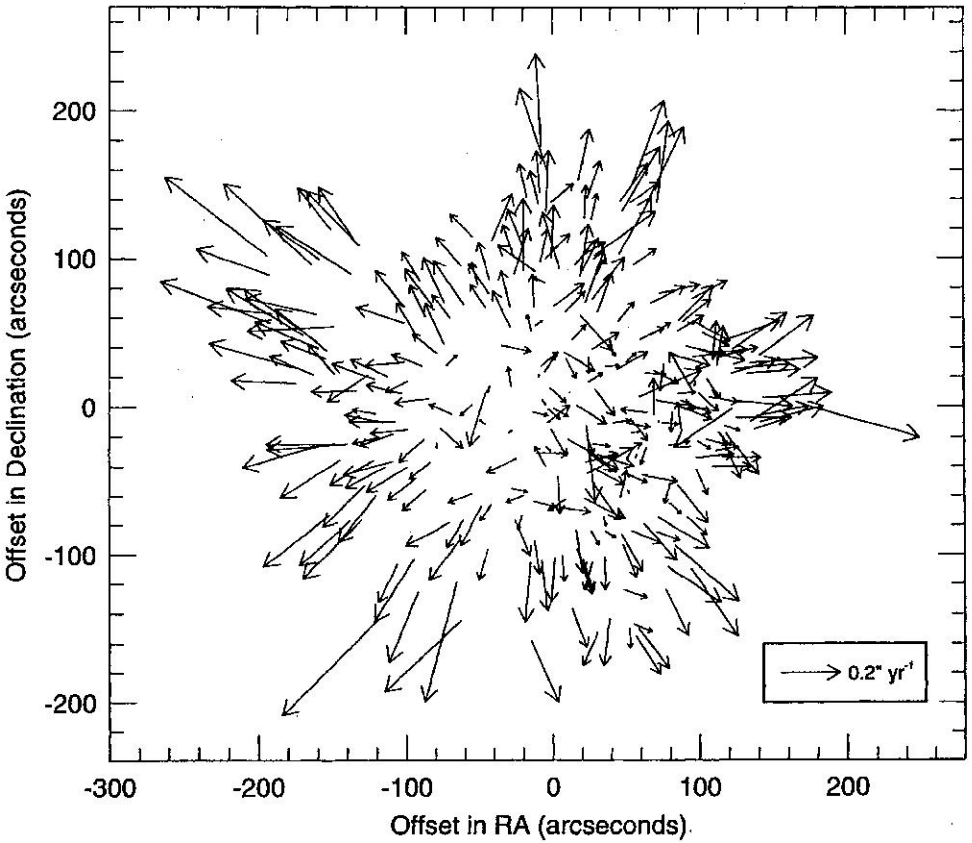

FIG. 4.—Proper motion vectors derived for 304 compact radio features in Cas A from 6 epoch linear positional fits. Position offsets are measured with respect to the radio knot expansion center.

Anderson, Rudnick (1995)

SPATIALLY RESOLVED POLARIZATION OF GALACTIC AND EXTRAGALACTIC X-RAY JETS

Kaaret et al. (2003)

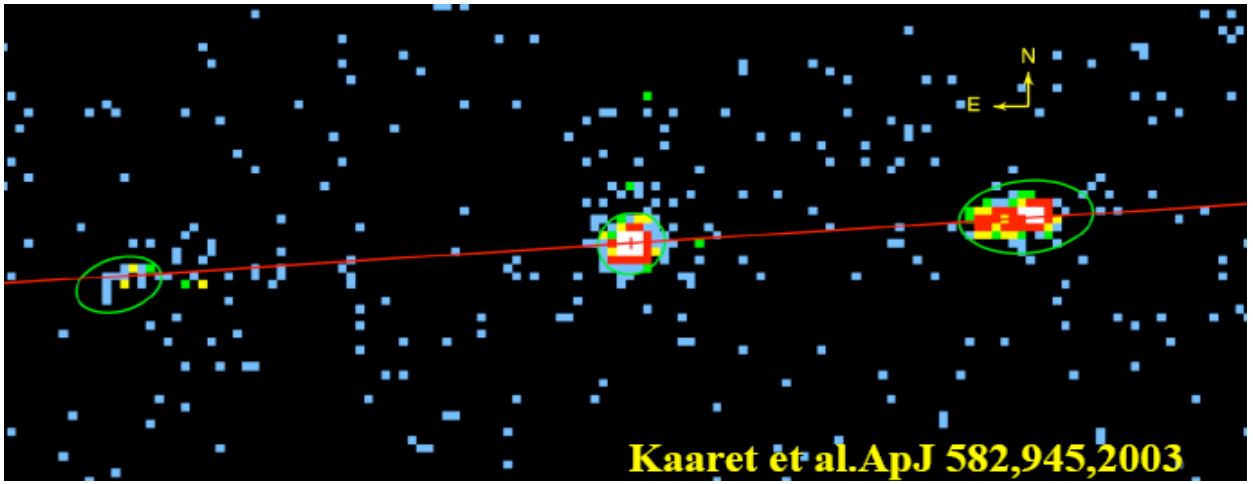

MDP 14 %

T= 10^5 s

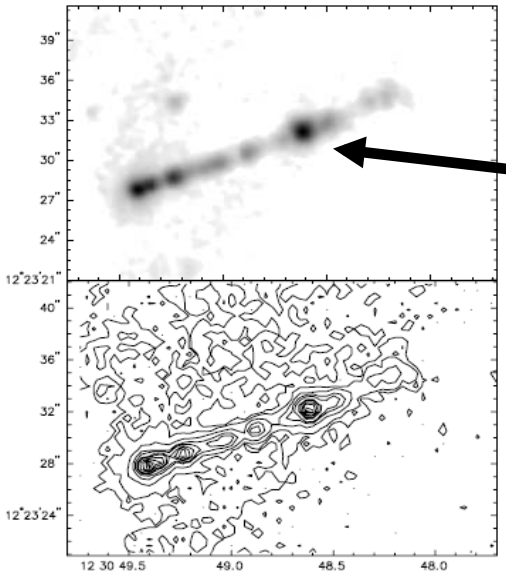

M87 MDP Knot A 5.3% in 10^5 s

Syncrotron or External Compton ?

AGNs

Cara et al. (2013)

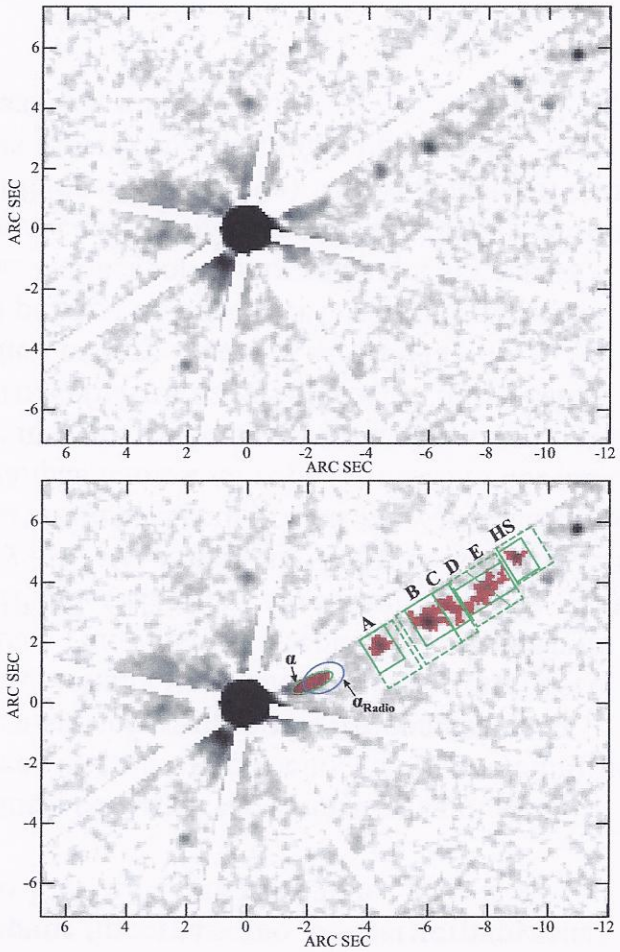

Figure 1. Galaxy subtracted HST F555W Stokes *I* image of the PKS 1136−135 jet, at top, and at bottom, with knot nomenclature and used apertures superposed. The white regions represent diffraction spike features that have been excluded from our analysis. Dashed green rectangles show the largest apertures. Solid green rectangles and ellipse show smaller apertures. These represent the regions within which pixels were considered for inclusion in various knot regions. The dotted green diagonal line separates knots D and E based on a radio image. The 1σ-cut apertures are shown as red masks overlaid on the jet knots. The blue ellipse shows the location of the knot α in the radio image. See §§ 2.4 and 3.1 for discussion.

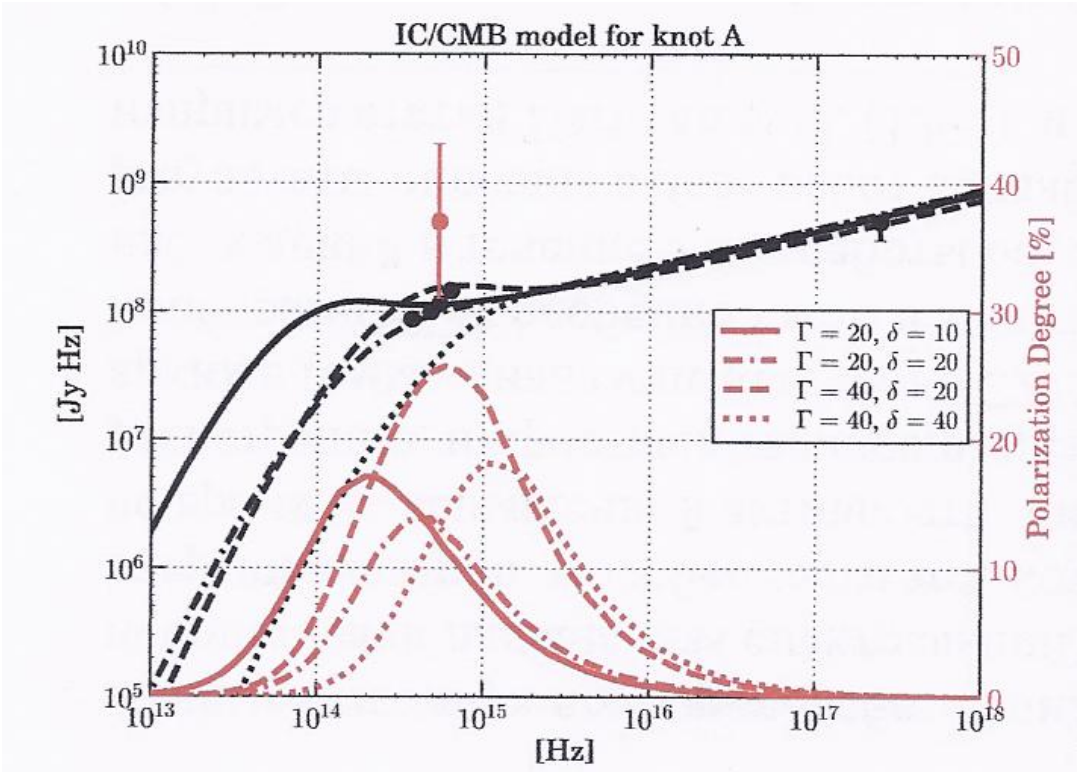

Figure 5. Intensity (black curves) and polarization degree (red curves) of the IC/CMB emission from a relativistic jet as a function of observing frequency. Data points present the *HST* results for knot A obtained in this paper. We show plots for jet bulk Lorentz factor $\Gamma = 20$ and 40, with beaming factor $\delta = \Gamma$ and $\delta = \Gamma/2$. See § 4.1 for discussion.

Polarimetry with Integral

1. Polarimetry with the Integral/SPI telescope (Dean et al. (2008));
2. Polarimetry with the Integral IBIS/Compton telescope (Forot et al. (2008));
3. Observation of variable polarization in GRB 041219A (McGlynn et al. (2007));
4. Constraints on LIV from GRB 041219A (Laurent et al. (2011)), from GRB 061122 observations (Goetz et al. (2013)), and from GRB 140206A (Goetz et al. 2014)

Crab Polarisation - Off pulse event selection

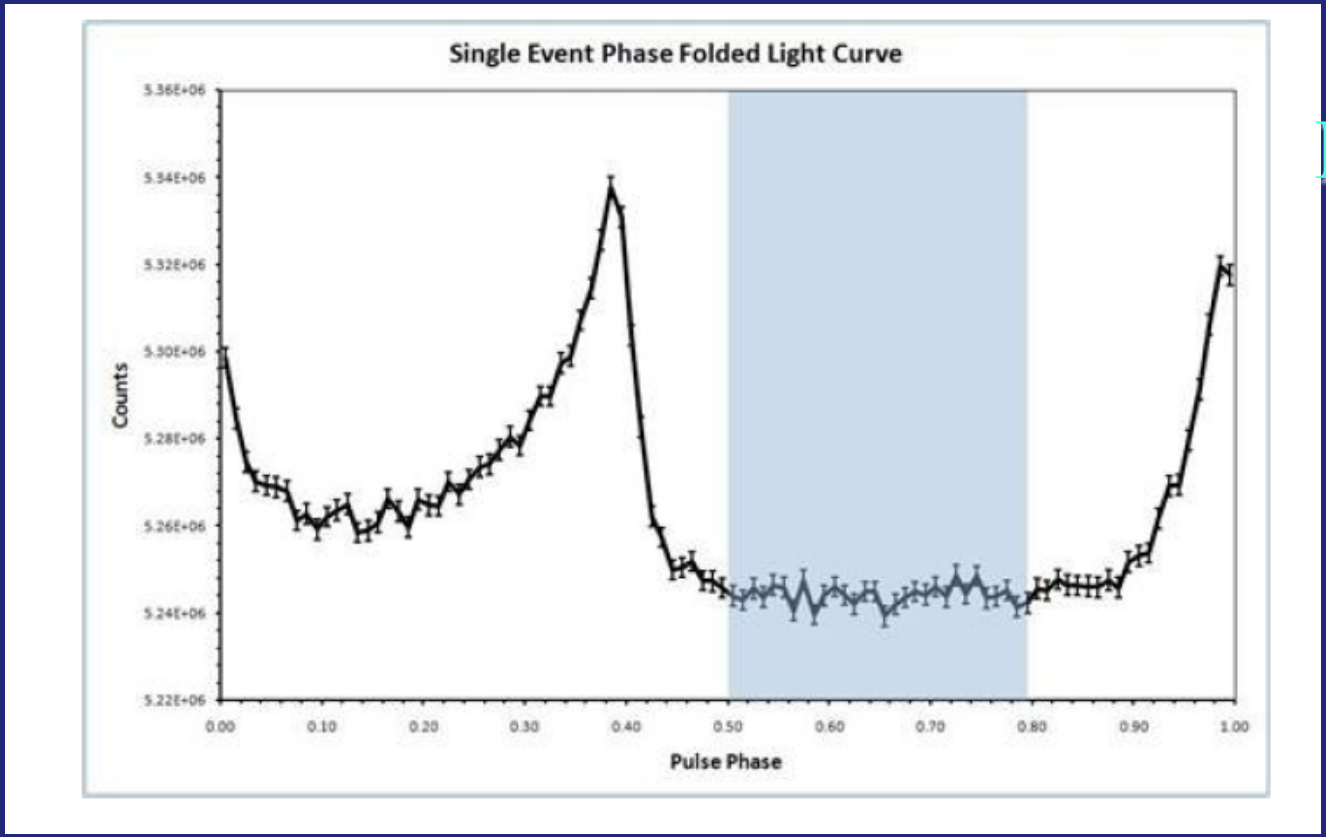

Dean (2008)

- *Double events (<350ns apart) selected from shaded region*
- *Phase interval 0.5 – 0.8 of the pulsar period*
- *Only events that occur in adjacent pixels were considered*
- *Events selected in the 0.1 – 1 MeV range*

Crab Polarisation - Polarisation Angle and % Polarisation

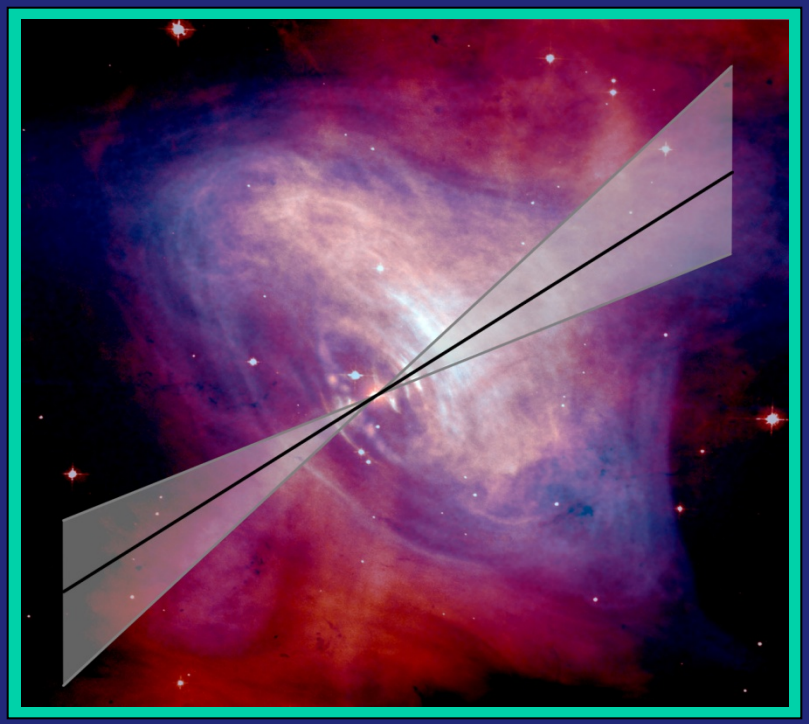

Dean (2008)

- *Unpulsed emission is highly polarised*
- *Electric vector : Light Grey represent errors*
- *Good alignment with inner jet structure*

- *Best fit angle = 123º ± 11º (from North, anticlockwise on sky)*
- *Best fit linear polarisation = 46% ± 10%*

Which model is correct?

Polar Cap	Outer Gap	Slot Gap

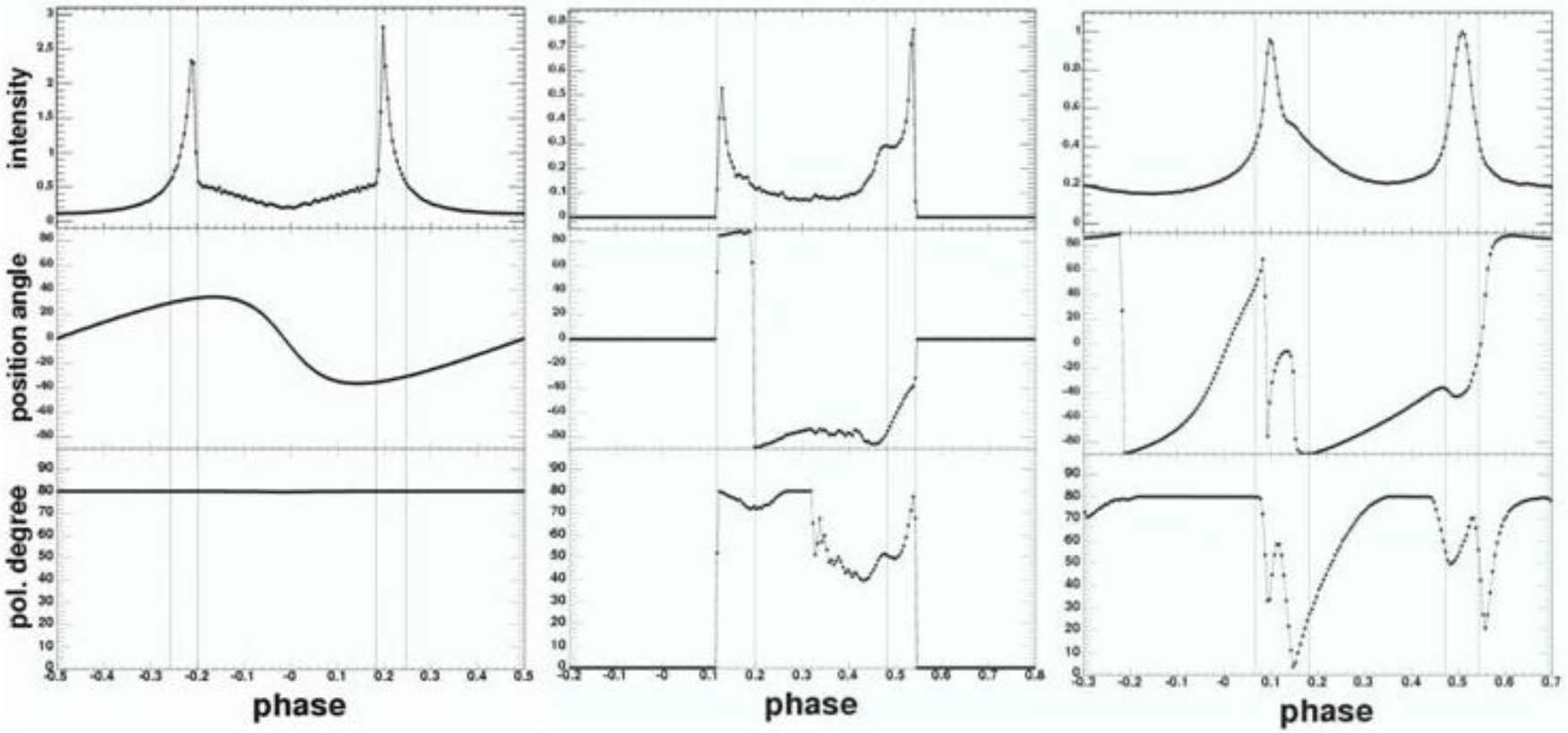

Daugherty & Harding	Romani & Yadigaroglu	Dyks et al.

Crab Pulsar polarization

- The Crab optical polarization degree (PD) is strongly phase-dependent (Wampler et al. 1969)
  - Low (~ 1%) in the Main Pulse (MP) and in the Inter pulse (IP)
  - Stronger (~20%) in the Bridge and maximum (~40%) in the Off-Pulse (OP)
- The polarization angle (PA) is phase-dependent too, with maxima lagging ~ 0.10 in phase the MP and the IP

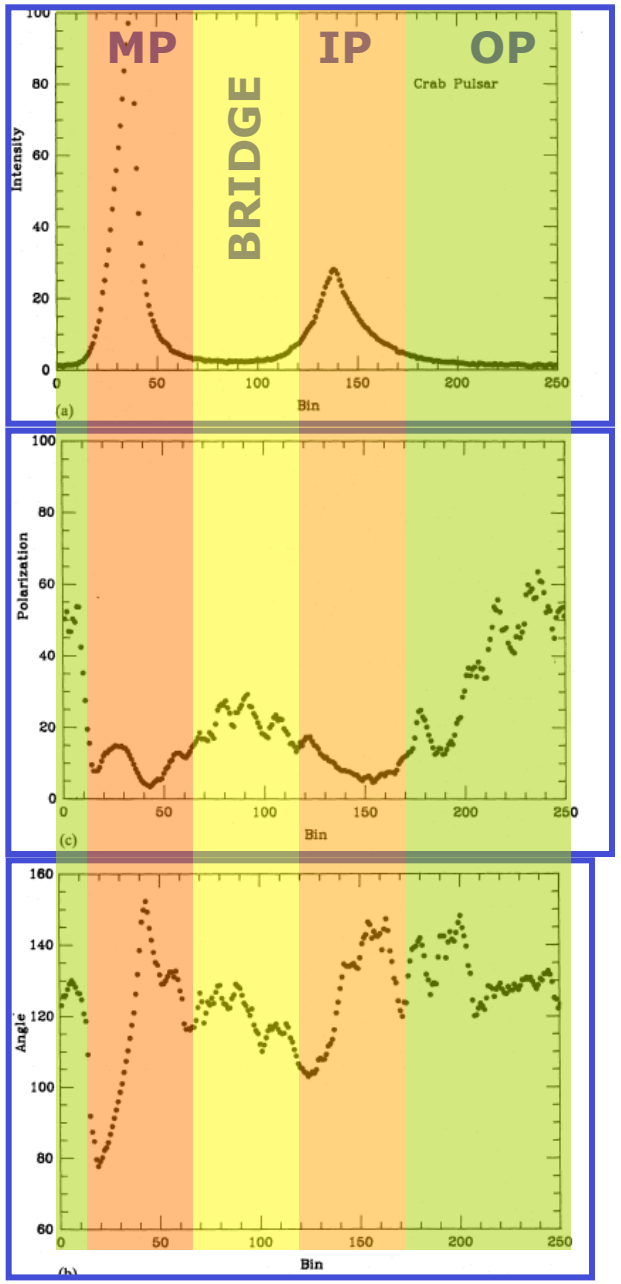

From Smith et al. (1988)

Comparison with pulsar models within the LC

Dean (2008)

Curvature radiation

Synchrotron radiation

Outer gap

Caustic model

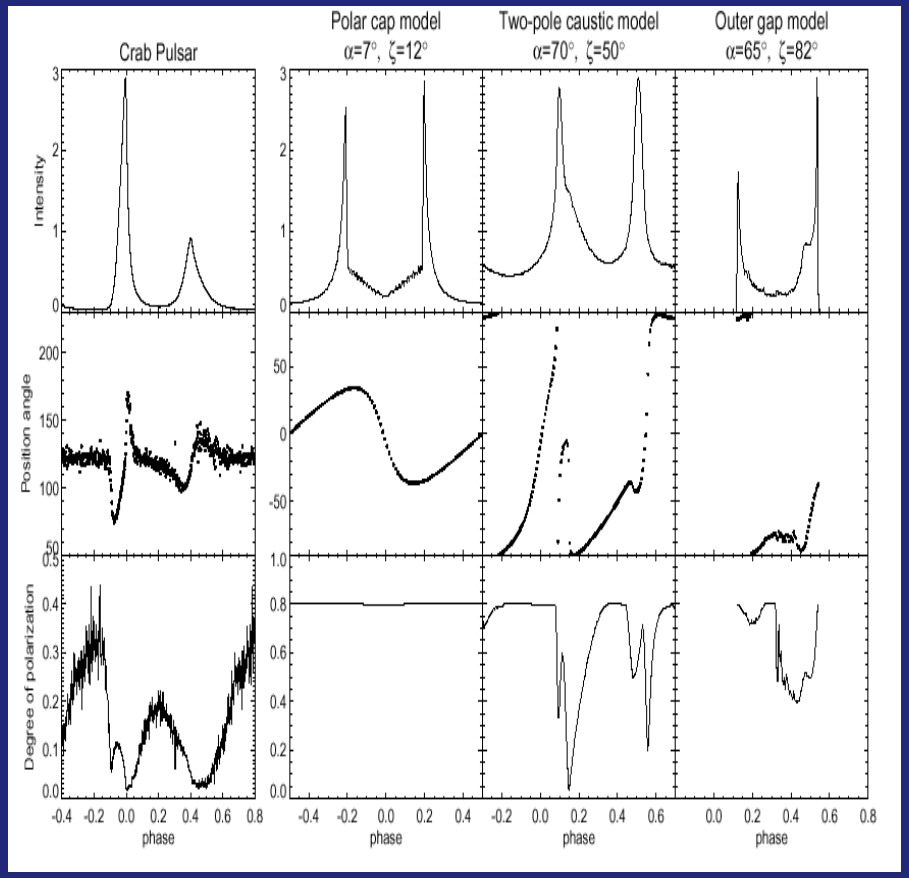

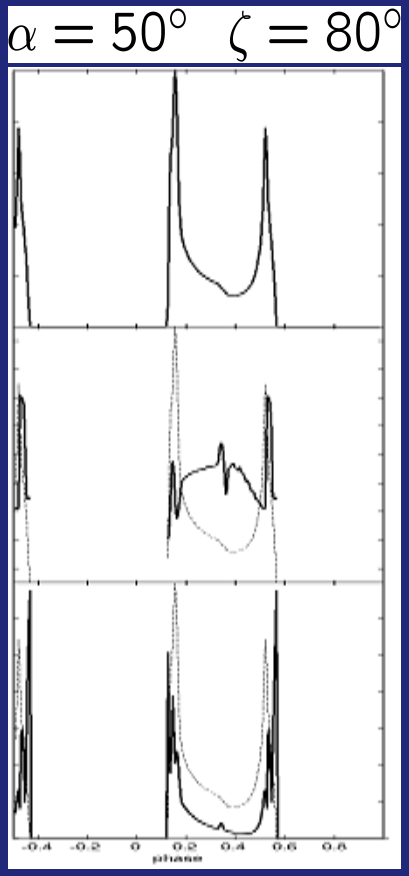

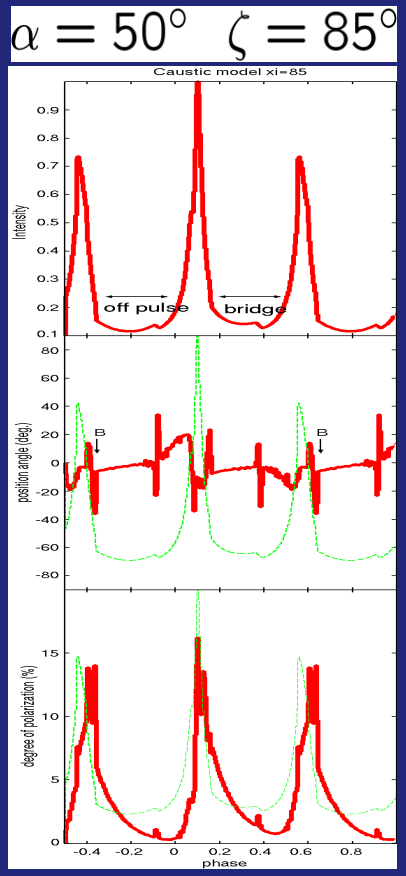

Taken from Takata, Chang & Cheng

Comparison with pulsar models

Dean (2008)

- *None of the pulsar models adequately predict a highly polarized off pulse component as seen by INTEGRAL.*

- *Total possibly superposition of 2 components. (e.g. Dyks, Harding & Rudak (2004); Takata, Chang & Cheng (2007)).*

- *High degree of γ-ray polarization & alignment with optical from central ~arcsec imply (offpulse) γ-rays come from well within X-ray ring (i.e. within termination shock) & wisps*

- *Hence the polarized offpulse component must come from structure(s) outside the light cylinder & within the termination shock. (inner jet, striped wind zone, hotspot/ knot(s)…)*

Crab

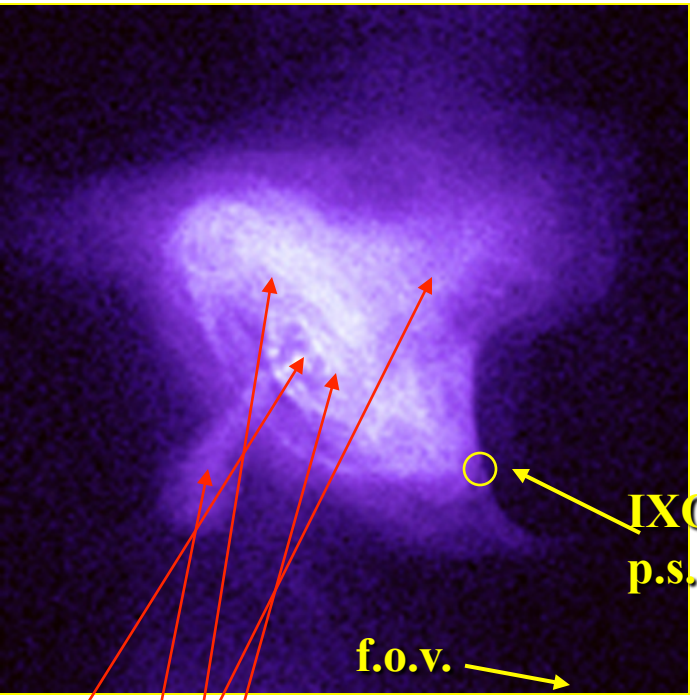

Positive measurement: of X-ray polarization of the Crab Nebula without pulsar contamination (by lunar occultation, Weisskopf et al., 1978).

$P = 19.2 \pm 1.0\ \%$

$\theta = 156.4^{o} \pm 1.4^{o}$

But this is only the average measurement The structure is much more complex!

Crab X-ray PSR polarization see Moran et al. (2013)

With XPOL, or similar, one can perform the separate polarimetry of details of the major structures to answer the questions, like:

How turbulent is the field?

How polarized is the PSR jets, wisps, knots?...

XPOL (IXO)—L. Piro (2008)

HST hotspot dynamical motions within jet (Dean (2008)

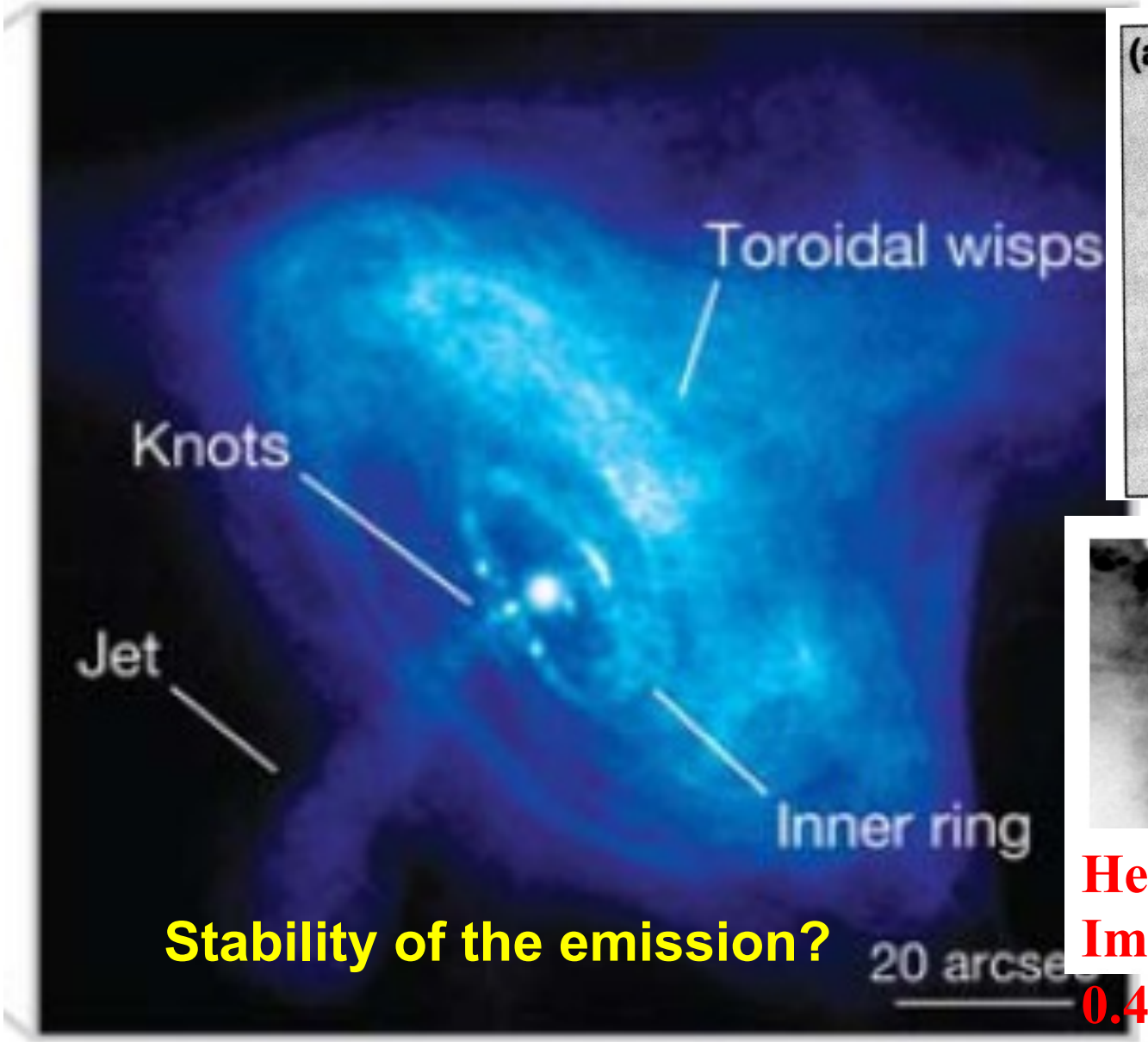

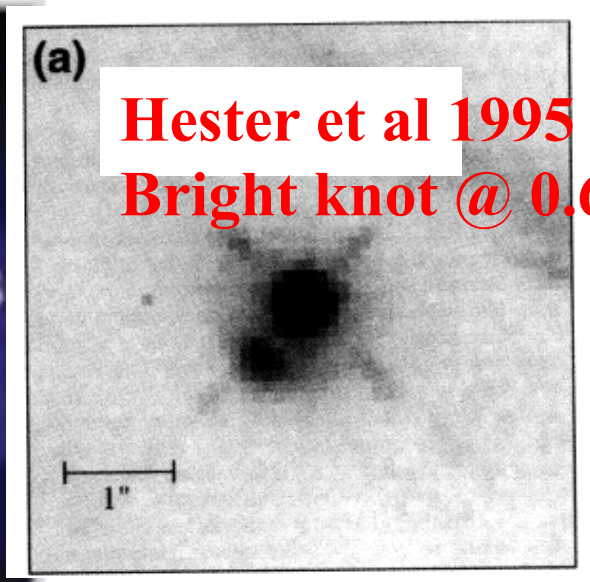

Hester et al 1995
Bright knot @ 0.6

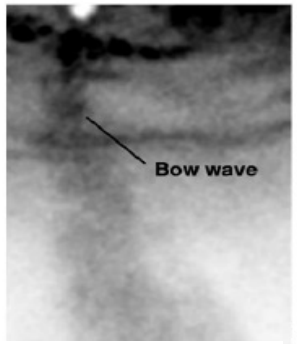

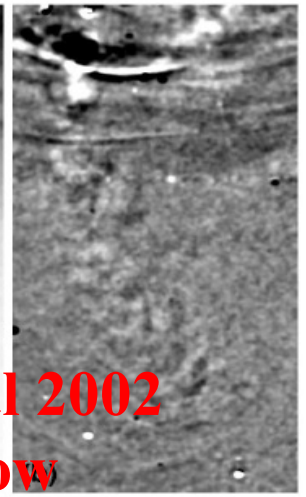

Hester et al 2002
Images show
0.4C motion ⇒

We need imaging X-ray polarimetry with good timing

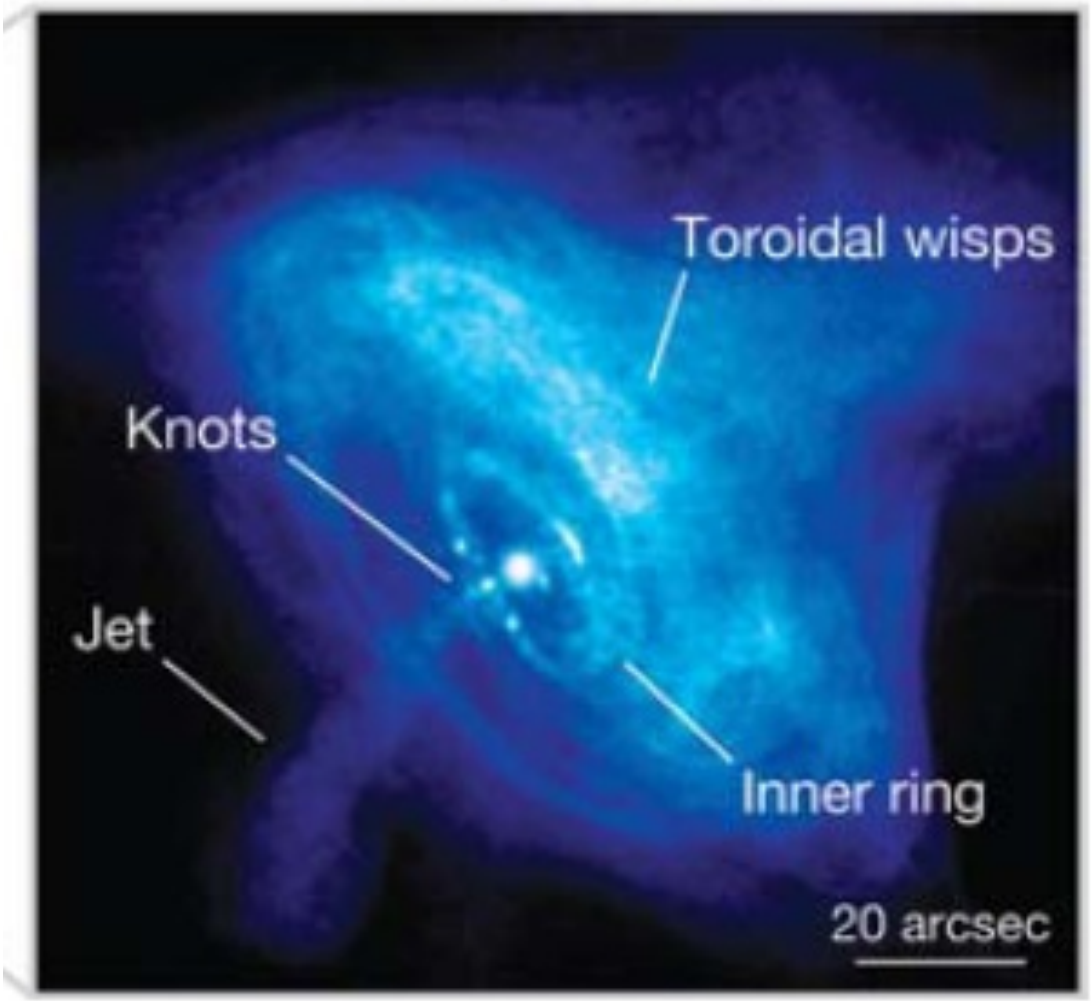

GRB polarization – what for?

- GRB collimated jet geometry and content.
- GRB jet magnetic structure
- GRB emission via shock(s)?
- GRB early afterglow polarization as a key ingredient to understand geometry of the jet;
- Lorentz Invariant Violation – vacuum birefringence (Fan et al. 2007; Laurent et al. (2011); Stecker (2011); Toma et al. (2012); Goetz et al. (2013)
- GRB 140206A => LIV -- $\xi < 10^{-16}$ (Goetz et al. 2014)

GRB polarization: few cases

- GRB 041219A was detected in December 2004 by the Integral Burst Alert System (IBAS).
- Longest and brightest GRB detected in the Integral FOV so far with variable polarization!
- The Integral Spectrometer (SPI) reported a high polarisation level (68 %) observed during the brightest part of this GRB (Mc Glynn et al., 2007)
- What if the P & PA usually varied during the GRB prompt phase?

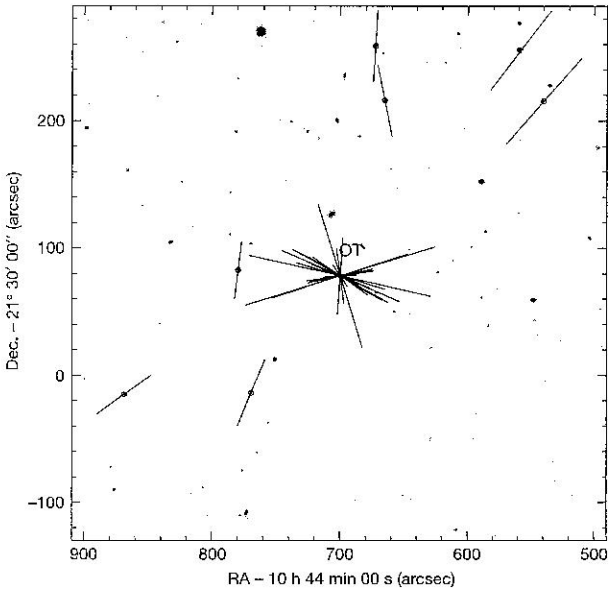

Figure 1 R band image of the field centred on the optical afterglow of GRB030329. The 27 FORS1 (Focal Reducer and Low Dispersion Spectrograph at the Very Large Telescope (VLT)/Antu) measurements are shown as 'vectors' where the length is a measure of the polarization degree, and the orientation indicates the position angle. While the afterglow varies in degree as well as angle, the polarization of seven field stars is constant within 0.1% in polarization degree and 1.5 degree in position angle throughout the 38 days. Linear polarization was measured from sets of exposures with different retarder-plate position angles. Imaging polarimetry was obtained during the first four nights (when the afterglow was brighter than 17th magnitude) from sixteen different retarder-plate angles, and from eight angles thereafter. Because the FORS1 polarization optics allows determination of the degree of polarization to an accuracy of $<3\times10^{-4}$ and of the polarization angle to ~0.2°, we consider the above variance of the field stars to represent the systematic error over the 38-day time period. Observations of polarimetric standard stars reproduced their tabulated values within 5%. The FORS1 retarder-plate zero-point angle of −1.2° was subtracted from the polarization angle. The position angle has a systematic uncertainty of ±1.5°, which was added in quadrature to the statistical errors. OT, optical transient.

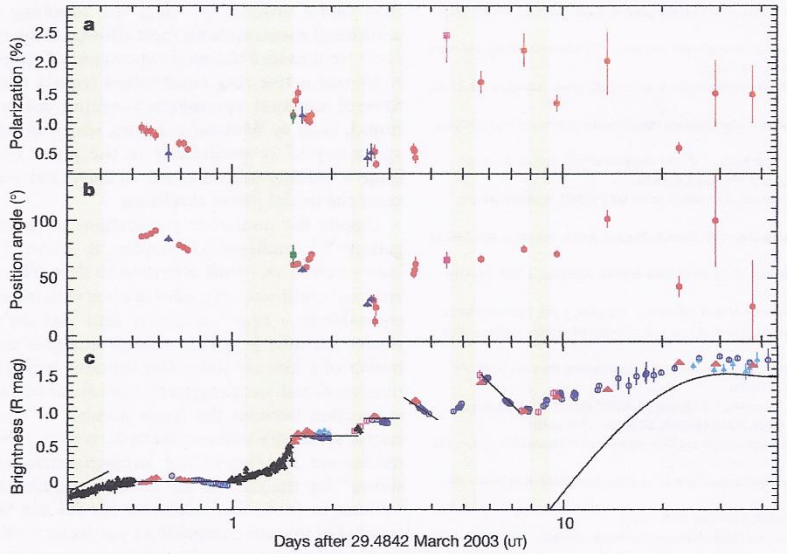

Figure 2 Evolution of the linear polarization during the first 38 days. **a**, **b**, The polarization degree in per cent and the position angle in degrees. The red data points are from imaging polarimetry with FORS1/VLT. Spectropolarimetry (blue symbols, 700–800 nm range) was performed during the first three nights. The green points were obtained with CAFOS at the 2.2-m telescope at Calar Alto on 30/31 March. The magenta data point was obtained with AFOSC at the 2.56-m NOT telescope on 2 April 2003. **c**, The residual R-band light curve after subtraction of the contribution of a power law $t^{-1.64}$ describing the undisturbed decay during the time interval 0.5–1.2 days after the γ-ray burst (that is, after the early break at 0.4 days), thus leading to a horizontal curve. The symbols correspond to data obtained from the literature (black), the 1-m USNO telescope at Flagstaff (blue), the OAN Mexico (light blue), and FORS1/VLT (red). Lines indicate phases of power-law decay, with the first one from early data[21] (not shown). Yellow bars mark re-brightening transitions. Contributions from an underlying supernova (solid curved line) do not become significant until ~10 days after the γ-ray burst.

Greiner et al., Nature (2003)

GRB's polarization

- GRB 041219A Π(68%)= 65+-26 % (IBIS).
- GRB 061122 Π(68%) > 60 % (IBIS)
- GRB 100826A Π(68%)= 25+-15 % (GAP)
- GRB 110301A Π(68%)= 70+-22 % (GAP)
- GRB 110721 Π(68%)= 84^{+16}_{-28} % (GAP)
- GRB 120711A Π(68%)= 54+-27 % (IBIS)
- GRB 140206A Π(68%) > 48 % (IBIS).

Compton polarimetry

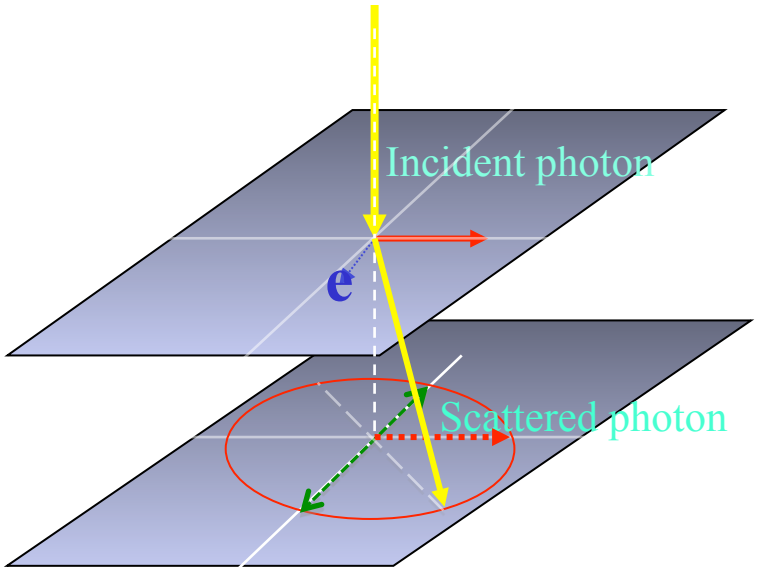

$$S = \bar{S}\left[1 + a.\cos(2(\varphi - \varphi_0))\right]$$

- Compton scattering cross section is maximum for photons scattered at right angle to the direction of the incident electric vector ⇒ asymmetry in the azimuthal profile S of scattered events.

- modulation
  - a = modulation factor
  - polar. fraction = PF = a/a_{100}
  - a_{100} = modulation for a 100 % polarized source.
  - polar. angle = PA = $\varphi_0 - \pi/2 + n\pi$

Note high level of Crab and Cyg X-1 polarization for hard X-rays

Conclusion

Compton-scatter type polarimeters are better suited for the hard X-ray range of AO's emission;
Imaging and high throughput are must;
TPC method for Compton polarimeter have to be studied in more detail;
Targets have to be chosen with a care;
Expectations have to be trimmed via simulations and calibrations
Do not forget to use spectral info

THANK YOU!